ACS OMEGA

Article

Cite This: ACS Omega 2018, 3, 10460−10470

http://pubs.acs.org/journal/acsodf

Novel ^{18}F-Labeled PET Imaging Agent FV45 Targeting the Renin−Angiotensin System

Xinyu Chen,[†,‡] Mitsuru Hirano,[∥] Rudolf A. Werner,[†,‡,⊥] Michael Decker,*[,§] and Takahiro Higuchi*[,†,‡,∥]

[†]Department of Nuclear Medicine, [‡]Comprehensive Heart Failure Center, University Hospital of Würzburg, Würzburg 97080, Germany

[∥]Department of Bio-Medical Imaging, National Cerebral and Cardiovascular Center, Osaka 565-0873, Japan

[⊥]The Russell H. Morgan Department of Radiology and Radiological Science, Division of Nuclear Medicine and Molecular Imaging, Johns Hopkins University School of Medicine, Baltimore, Maryland 21205, United States

[§]Institute of Pharmacy and Food Chemistry, University of Würzburg, Würzburg 97074, Germany

Supporting Information

ABSTRACT: Renin−angiotensin system (RAS) plays an important role in the regulation of blood pressure and hormonal balance. Using positron emission tomography (PET) technology, it is possible to monitor the physiological and pathological distribution of angiotensin II type 1 receptors (AT_1), which reflects the functionality of RAS. A new ^{18}F-labeled PET tracer derived from the clinically used AT_1 antagonist valsartan showing the least possible chemical alteration from the valsartan structure has been designed and synthesized with several strategies, which can be applied for the syntheses of further derivatives. Radioligand binding study showed that the cold reference FV45 (K_i 14.6 nM) has almost equivalent binding affinity as its lead valsartan (K_i 11.8 nM) and angiotensin II (K_i 1.7 nM). Successful radiolabeling of FV45 in a one-pot radiofluorination followed by the deprotection procedure with 21.8 ± 8.5% radiochemical yield and >99% radiochemical purity (n = 5) enabled a distribution study in rats and opened a path to straightforward large-scale production. A fast and clear kidney uptake could be observed, and this renal uptake could be selectively blocked by pretreatment with AT_1-selective antagonist valsartan. Overall, as the first ^{18}F-labeled PET tracer based on a derivation from clinically used drug valsartan with almost identical chemical structure, [^{18}F]FV45 will be a new tool for assessing the RAS function by visualizing AT_1 receptor distributions and providing further information regarding cardiovascular system malfunction as well as possible applications in inflammation research and cancer diagnosis.

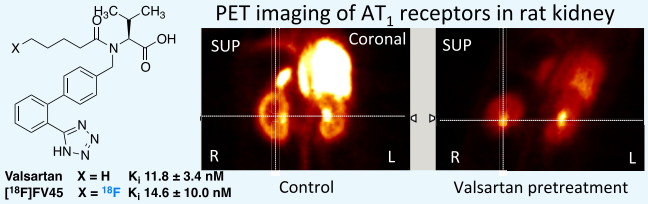

INTRODUCTION

The renin−angiotensin system (RAS) is a hormonal cascade that generates angiotensin peptides and is the main regulator of blood pressure as well as fluid and electrolyte balance.[1] The key mediator is the octapeptide angiotensin II, which stimulates mainly angiotensin II type 1 receptor (AT_1), a G-protein coupled receptor, and thereby initiates further downstream effects and leads to vasoconstriction. AT_1 receptors are mainly located in the heart, blood vessels, and kidneys. Therefore, it is currently one of the major therapeutic targets in the treatment of hypertension and heart failure (HF).[2] Furthermore, the angiotensin receptor/neprilysin inhibitor combination valsartan/sacubitril (LCZ696) has shown improved cardiovascular outcomes than ACE inhibitor enalapril as achieved in the prospective comparison of ARNI with ACEI to determine impact on global mortality and mobility in heart failure.[3] Its approval (commercial name Entresto by Novartis) for the treatment of HF in both the United States and Europe is considered a further milestone for the application of AT_1 antagonists.

In addition to the central role of RAS in the regulation of cardiovascular system mentioned above, it is also involved in a much broader range of functions in the body, including actions on growth factors, inflammation, mitosis, and cancer pathogenesis.[4] The majority of these functions are through the regulation of AT_1 receptors. Several clinical investigations involving a large number of patients in recent years have been conducted to explore the possibility of using AT_1 antagonists against several forms of cancer, e.g., prostate,[5] lung,[6,7] colon,[8] and breast cancer.[9] However, it should be mentioned that the results obtained remain controversial and the mechanism of these antitumor functions is not yet clarified. Studies have suggested that AT_1 receptor level changes during disease progression, while AT_1 blockade seems to be able to adjust the consequences of such alterations.[10−12] Therefore, AT_1 level is considered a key reflector of RAS function. Molecular imaging

Received: August 3, 2018
Accepted: August 14, 2018
Published: September 4, 2018

DOI: 10.1021/acsomega.8b01885
ACS Omega 2018, 3, 10460−10470

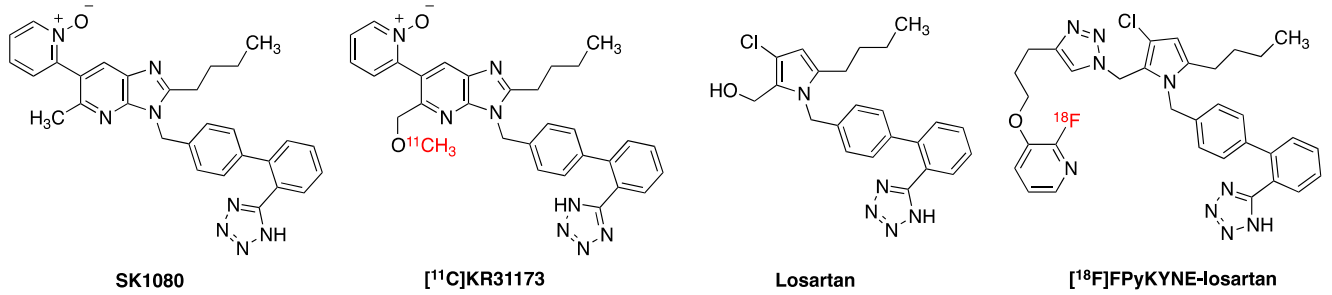

Figure 1. Chemical structures of currently reported AT_1 antagonist-derived radiotracers and their corresponding lead compounds.[18,22]

technique is ideal for monitoring in vivo AT_1 levels noninvasively. There is a high density of AT_1 receptors in the kidneys responsible for the regulation of blood pressure and furthermore functions.[13] Thereby, in animal studies, the kidney represents the primary organ of RAS imaging to be investigated.

In contrast to anatomical techniques, molecular imaging techniques using radionuclide tracers focus more on subcellular down to molecular-level events. They provide a noninvasive method to examine functional changes in individual organs, with high sensitivity, specificity, and the possibility of quantifying alterations. Moreover, the rational design of radiotracers based on biological and chemical knowledge makes it feasible to bring forth valuable pathophysiological information in patients and further insight into in vivo conditions of specific targets.[14] Currently, positron emission tomography (PET) is receiving more attention due to several advantages compared to single-photon emission computed tomography, namely, its higher count sensitivity, higher temporal and spatial resolution, as well as its ability to be used in dynamic and quantitative studies.[15] In PET applications with the possibility of performing dynamic and quantitative studies, new fluorine-18-based radiotracers bring forth improved imaging characteristics over carbon-11-labeled counterparts.[16] The use of fluorine-18 compensates the high cost for on-site radioisotope production due to its reasonably longer half-life (110 min) over carbon-11 (20 min), which has been one of the factors limiting the wide utilization of PET. This allows multiple scans each day with barely any in-patient cost. Besides, the application of fluorine-18 in PET may also provide higher flexibility in the design and syntheses of novel PET tracers together with an improvement of in vivo stability by reduced metabolism.[14]

Considering the important role of the RAS regulation of the renal and cardiovascular system and the necessity of clarifying its role in inflammation and tumor pathophysiology, PET tracers derived from highly selective AT_1 specific antagonists are of interest and ideal to reflect its levels, especially in functional diagnosis of renal and cardiovascular diseases or hallmarks of cancer.[17] To date, the application of such tracers in PET imaging has not yet been extensively investigated, and only a handful of radiotracers (Figure 1) have been reported: [^{11}C]KR31173, the methoxy analogue of the nonpeptide AT_1-selective antagonist SK1080,[18−20] and ^{11}C- and ^{18}F-labeled losartan derivatives connecting the sartan moiety with the radioactive fluoropyridinyl moiety using click chemistry.[21−26]

By applying [^{11}C]KR31173 (Figure 1), it was possible to establish first correlations between arterial and kidney blood input and radioligand uptake in pigs, which makes it a candidate for quantitative evaluation of RAS functions in this organ.[27,28] Recently, the first-in-human study has also been approved and performed, which showed good clinical safety along with detectable and specific myocardial retention.[29] However, it should be pointed out that even though [^{11}C]KR31173 has the above-mentioned properties, the clinical application might be limited due to the general drawbacks of ^{11}C-labeled tracers as mentioned above.

A fluorine-18-labeled losartan tracer was derived from its corresponding short-half-life carbon-11 tracer.[25] [^{18}F]-FPyKYNE-Losartan (Figure 1) was successfully labeled using click chemistry. Its in vivo studies on rats and pigs have been performed with favorable binding profile.[26] In addition, this tracer seems to make in vivo quantification of kidney AT_1 receptors possible in the process of disease development and applied pharmacotherapies.[30] Yet, compared to either losartan or candesartan, high liver uptake and decreased angiotensin II pressor effect at AT_1 receptor might be drawbacks, possibly due to the introduction of bulky triazole and pyridine moieties in favor of easy labeling procedure. In addition, the multi-step radiolabeling procedure as well as the decrease of binding affinity to AT_1 receptor might also limit the application.

Valsartan shows high efficacy, tolerability, and patient compliance, which make it one of the leading antihypertensive and cardioprotective therapeutics.[31] The advantage of using valsartan as the lead structure to develop an ^{18}F-labeled tracer for PET imaging is based on its comparatively simple chemical structure and hydrophilicity, which might lead to relative lower liver uptake and therefore better imaging quality. Furthermore, deriving the radiotracer from a reference drug may reduce the cost of production by using the same chemical intermediates for preparation. By investigating the structure−activity relationships (SARs) of the sartan series of compounds, fluorine-18 can be introduced into the terminal of its aliphatic "tail". Thereby, a novel tracer [^{18}F]FV45 targeting RAS was designed (Figure 2). A substituent on the diphenyl ring will lead to increased binding affinity at AT_2 receptors.[32] An introduction of fluorine on the isopropyl moiety is another possibility, although the synthetic

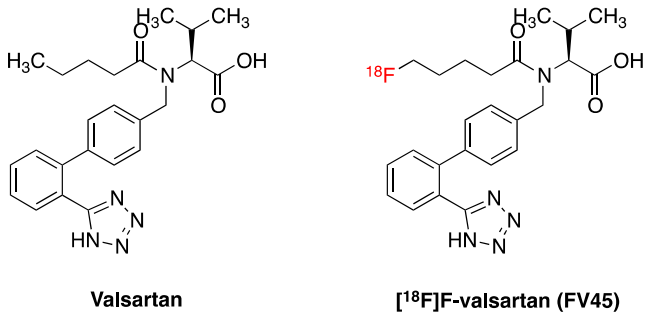

Figure 2. Chemical structures of valsartan and the proposed ^{18}F-labeled radiotracer [^{18}F]FV45.

DOI: 10.1021/acsomega.8b01885
ACS Omega 2018, 3, 10460−10470

Scheme 1. Synthetic Scheme of Biphenyl Tetrazole Moiety 4[35,36]

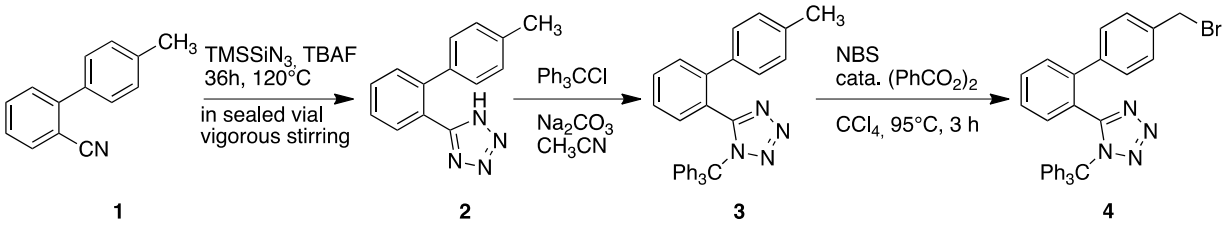

Scheme 2. Synthetic Attempts for the Preparation of Cold Compound FV45 and the Precursor for Radiolabeling[37,38]

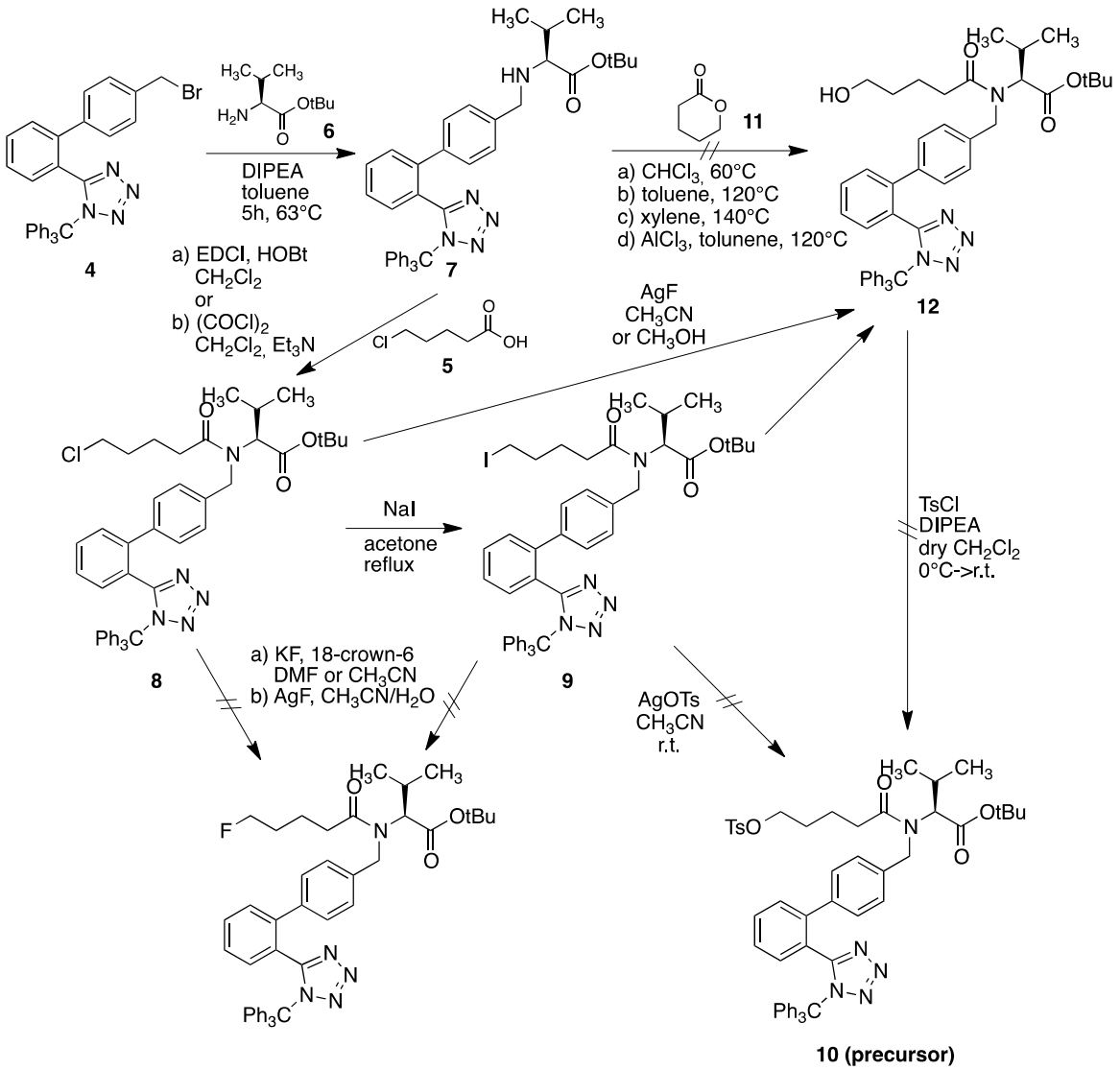

approach to achieve a corresponding precursor (on which the radioactive isotope is introduced to form the target radioactive tracer) would be chemically demanding. Since fluorine is smaller than hydrogen and has neutral properties, this modification should maintain its affinity and give access to a comparatively straightforward chemical synthetic scheme.[33] In addition, fluorination on this position might block the formation of a potential metabolite, nonactive 4-hydroxyvalsartan,[34] and consequently, alter the pharmacokinetics of this tracer, for instance, by decreasing liver uptake and increasing renal excretion.

RESULTS

Chemistry. To prepare the precursor for labeling, different synthetic approaches have been investigated for the preparation of both the precursor and the corresponding cold compound (nonradioactive fluorine derivate). Diphenyl tetrazole moiety **4** was prepared according to the procedure described in the literature (Scheme 1).[33,35]

In the first attempt to build the precursor, 5-chlorovaleric acid **5** was attached to the diphenyl valinate moiety **7**, which was formed by reacting diphenyl tetrazole moiety **4** with *tert*-butyl valinate **6**. The chlorine atom in compound **8** was replaced by iodine through the Finkelstein reaction. While trying to

DOI: 10.1021/acsomega.8b01885
ACS Omega 2018, 3, 10460−10470

Scheme 3. Final Synthetic Schemes of Precursor 10 with Corresponding Cold Reference FV45 and Radiolabeling Procedure

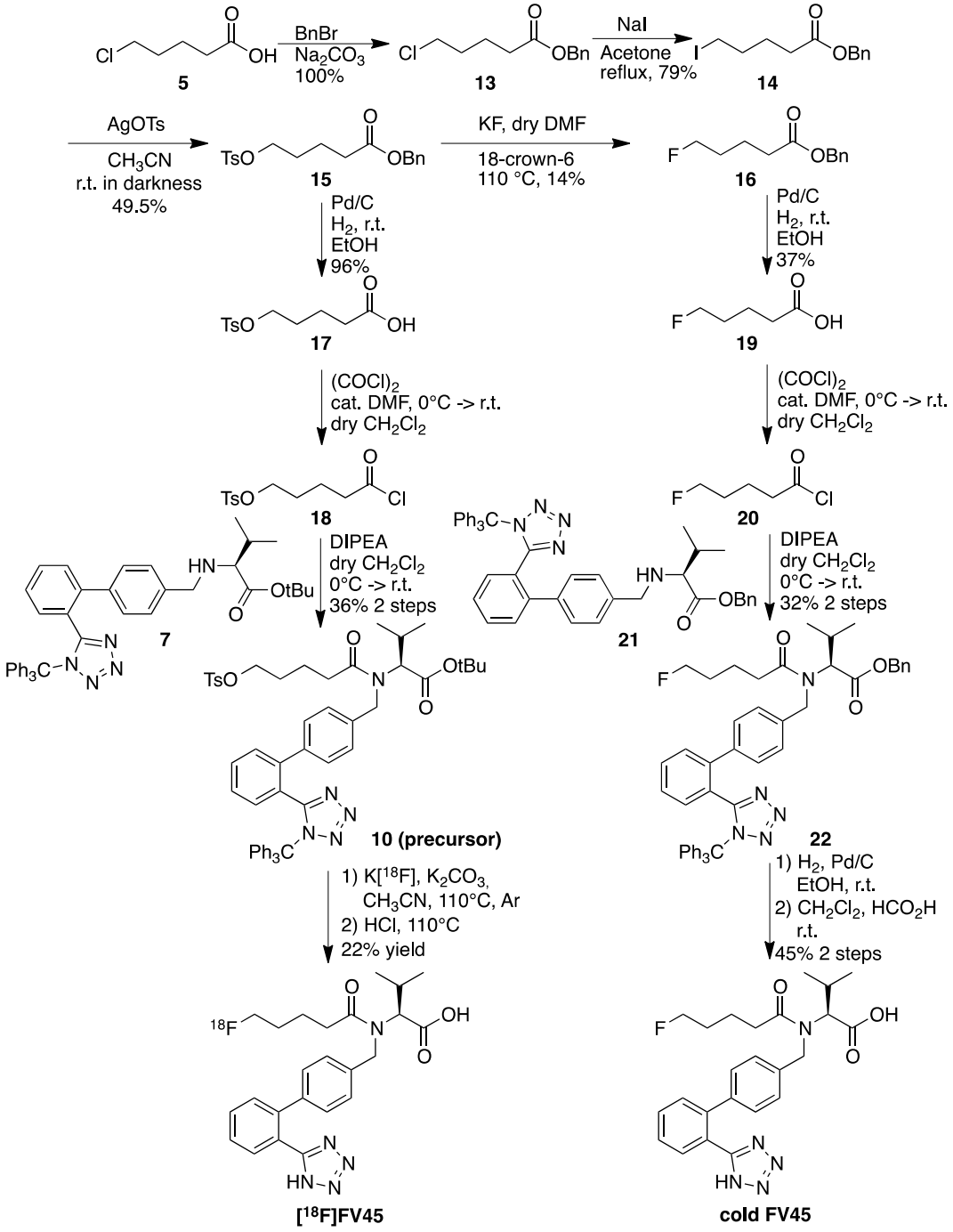

introduce a tosylate moiety into compound **9** to serve as a leaving group for fluorination, the *p*-toluenesulfonic acid in silver tosylate leads to deprotection of the trityl group of the tetrazole and no product **10** was formed. The reaction could not take place either when adding 10% base in the attempt to neutralize excessive acid. Subsequently, a second attempt to achieve *ω*-hydroxyvalsartan **12** was performed by reacting the diphenyl valinate moiety **7** with *δ*-valerolactone **11** in different solvents, including chloroform, toluene, and xylene, at various temperatures. However, none of them gave desired products. While using aluminum chloride-catalyzed ammonolysis of compound **7** with lactone **11**,[37] the starting material decomposed in the reaction condition with no product formation. Using silver fluoride in an effort to replace either chloride of compound **8** or iodide of compound **9** also turned out to be unsuccessful and produced mainly *ω*-hydroxyvalsartan **12**.[38] Unfortunately, an attempt to react this byproduct compound **12** with tosyl chloride to get the precursor **10** failed, too. All unsuccessful attempts to achieve precursor and cold compound are illustrated in Scheme 2.

The final synthetic procedure used the acyl chain with either fluorine (for the cold reference) or tosylate (for the precursor) already connected, followed by coupling with the diphenyl valinate moiety **7**. Accordingly, the successful approach started from 5-chlorovaleric acid **5**, which was first esterified to protect the carboxyl group. The chlorine atom in compound **13** was

DOI: 10.1021/acsomega.8b01885
ACS Omega 2018, 3, 10460−10470

replaced by iodine through the Finkelstein reaction. This gave the possibility of further replacement by tosylate using silver tosylate, which was obtained by mixing equal molar quantities of silver oxide with 4-toluenesulfonic acid in acetonitrile in darkness.[39] After removal of the benzyl ester selectively under mild hydrogenation conditions without affecting the tosylate, acid **17** reacted with oxalyl chloride in dry dichloromethane to form acid chloride **18**. It was then reacted with diphenyl valinate moiety **7**, and precursor **10** became available for labeling (Scheme 3). The fluorine atom of the cold compound was introduced by replacing the tosyl in intermediate **15**.[40] Fluorination conditions could also be evaluated as a reference for the radiolabeling procedure. Thereafter, FV45 was synthesized analogously as the precursor, with the only difference of using benzyl valinate **21** instead of *tert*-butyl ester (Scheme 3). The benzyl ester group is more stable during preparation, whereas *tert*-butyl ester in the precursor could be concomitantly removed after radiolabeling together with the trityl group under acidic condition.

Radiochemistry. As a good leaving group, a tosyl moiety could be substituted by fluorine-18 in the labeling procedure. Different solvents, reacting temperature, and sources of $[^{18}F]F^-$ were investigated. Dimethylformamide (DMF) provided high reaction temperature up to 140 °C. Acetonitrile gave mild reaction condition and temperature and is also easier to provide anhydrous condition by azeotropic distillation. In addition, $Cs[^{18}F]F$, $K[^{18}F]F$ and tetrabutylammonium $[^{18}F]F$ ($[^{18}F]$TBAF) were used as sources of fluorine-18. Although all of these sources and conditions succeeded in radiolabeling, $K[^{18}F]F$ in acetonitrile with $Kryptofix_{2.2.2}$ as phase transfer catalyst was selected as the most conventional and conveniently performed procedure. The last step, deprotection of both trityl on tetrazole and *tert*-butyl ester group, was first set for 10 min at 110 °C. During the purification via semipreparative high-performance liquid chromatography (HPLC), the formation of a 30−50% of byproduct was observed. This byproduct was later identified as the *tert*-butyl ester of FV45 (Figure S2). As it had turned out that the *tert*-butyl ester is more stable than expected, the reaction time for deprotection was prolonged to 20 min. The intermediate was then also transformed to the target tracer, and the yield for $[^{18}F]$FV45 was greatly improved (Figure S3). Finally, a purification step using semipreparative HPLC was still needed since the majority of the precursor decomposed during radiofluorination procedure and a couple of byproducts formed that could not be simply removed with a C18 Sep-Pak. In the end, with the improved labeling condition and procedure, the total synthesis of labeling takes approximately 120 min. The average overall radiochemical yield was 21.8 ± 8.5% (decay-corrected based on the starting radioactivity, calculated from 5 times of labeling records), and radiochemical purity was >99%. In summary, with one-pot reaction and straightforward labeling procedure, the rationale of the tracer design was successfully achieved. Additionally, such procedure would be easily scaled up for further preclinical or even clinical studies, with the possibility of using fully automated labeling system for tracer synthesis.

Binding Studies on Human AT_1 Receptors. To evaluate the binding affinity of FV45 at AT_1 receptors, it is necessary to compare the cold reference with both its lead valsartan and angiotensin II. By doing so, it would be able to confirm that such strategy of designing tracers from the corresponding clinically used drug is principally feasible. It would also provide further insight into the strategy, whether the introduction of fluorine at the terminal of the acyl chain would affect the binding affinity of FV45 to AT_1 receptors. Although fluorine is considered as a bioisostere of hydrogen, it is also possible to behave as a hydrogen-bond acceptor.[41] In short, membrane from CHO-K1 cells expressing human AT_1 receptors were used in the assay. Competitive binding of angiotensin II, valsartan, and FV45 was tested against ^{125}I-angiotensin II as the radioligand. The results clearly showed that FV45 could compete with the radioligand to bind to AT_1 receptors in a concentration-dependent manner (Figure 3). It has proved that the derivation did not affect the

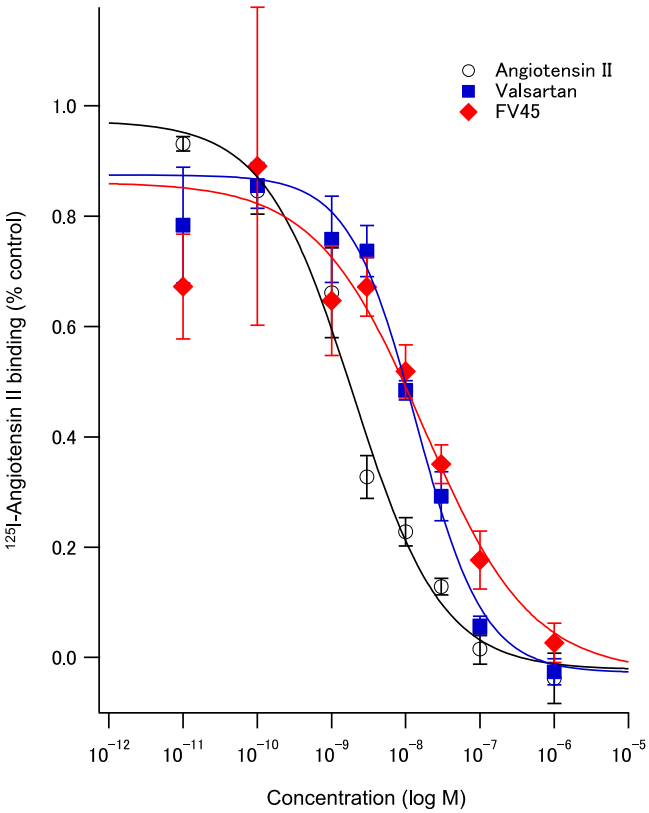

Figure 3. Competition experiments of ^{125}I-angiotensin II binding to a membrane preparation from CHO-K1 cells expressing the human AT_1 receptor. Sigmoidal curves for concentration-dependent inhibitory effects of angiotensin II (black circle), valsartan (blue square), and cold FV45 (red diamond). Data are mean ± standard deviation from four independent experiments. The K_i values are 1.7 ± 0.4 nM for angiotensin II, 11.8 ± 3.4 nM for valsartan, and 14.6 ± 10.0 nM for FV45.

competitive binding affinity of FV45, which retained in the same range as its lead valsartan (K_i value FV45 14.6 nM vs valsartan 11.8 nM), while slightly less compared to angiotensin II (1.7 nM). The almost identical affinity profile enables the application of our synthesis procedure to other sartans with similar structures to derive corresponding tracers or to develop further sartan derivatives for therapeutic purposes, for instance, to change bioavailability or pharmacokinetics.

Renal Imaging Studies in Rats. Standard protocols and data analysis methods for noninvasive PET imaging of small animals have been well established in our working group.[42] After $[^{18}F]$FV45 was successfully labeled as described above and radioactive purity was confirmed, the anesthetized rats of the control group were injected the tracer via the tail vein. To determine the specificity of $[^{18}F]$FV45, the rats were first treated with AT_1 antagonist valsartan 10 min before the tracer was

DOI: 10.1021/acsomega.8b01885
ACS Omega 2018, 3, 10460−10470

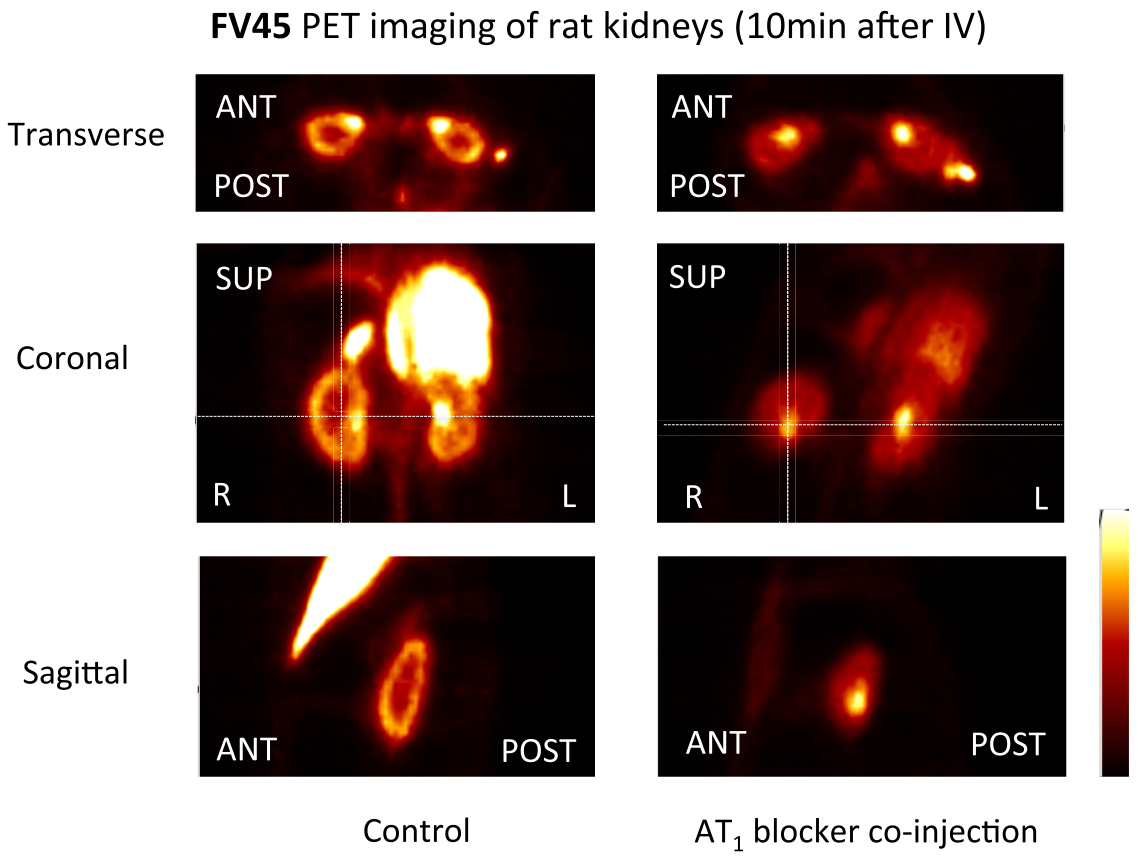

Figure 4. Kidney uptake of [^{18}F]FV45 as control (left) and blockade by selective AT_1 antagonist valsartan (right). Preadministration of AT_1 antagonist valsartan distinctly inhibits the kidney coronal uptake of this derived tracer [^{18}F]FV45.

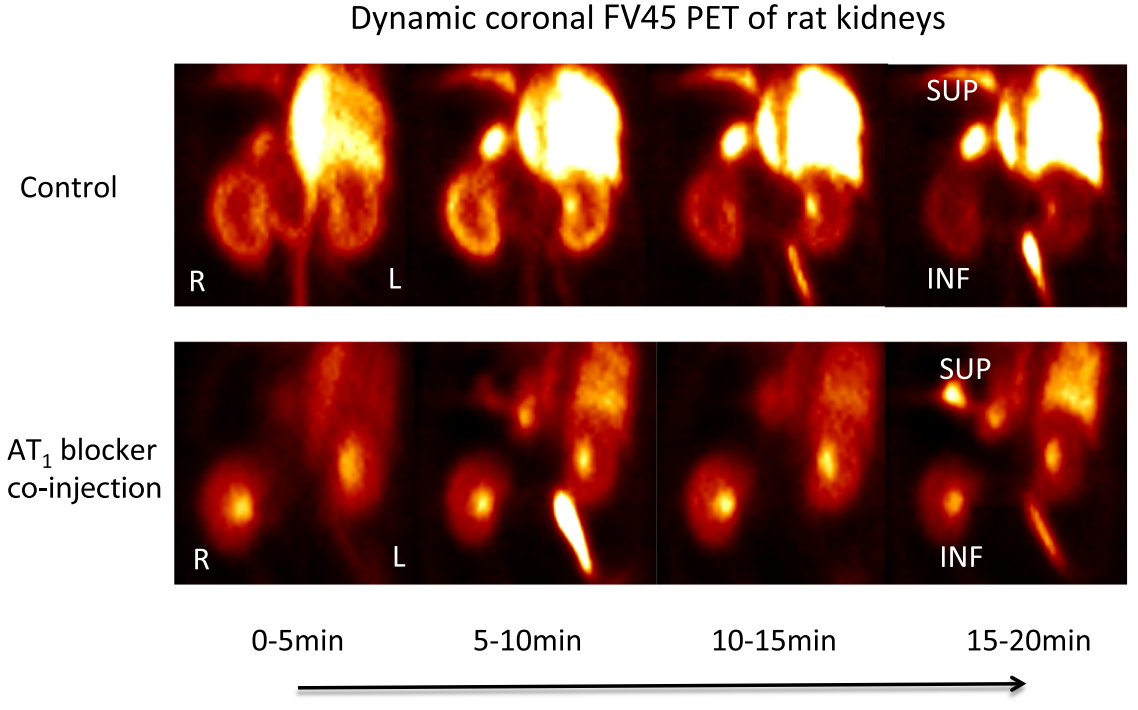

Figure 5. Dynamic coronal uptake of [^{18}F]FV45 as control (top) and blockade by selective AT_1 antagonist valsartan (bottom). Every 5 min is a time frame. Co-injection of AT_1 antagonist valsartan clearly reduced the kidney uptake of [^{18}F]FV45 that shows a selective AT_1 receptor-targeting mechanism.

administered. A 60 min list-mode PET acquisition focusing on the kidney area was started shortly after the injection because there is high density of AT_1 receptors expressed in the kidney. The static images obtained demonstrated distinct [^{18}F]FV45

DOI: 10.1021/acsomega.8b01885
ACS Omega 2018, 3, 10460−10470

accumulation in the kidneys, mainly renal cortex. Valsartan visibly inhibited kidney uptake of [^{18}F]FV45 (Figure 4), which indicates that the tracer uptake is specific to the AT_1 receptor. Further dynamic imaging of the tracer revealed that there was a fast and high uptake of [^{18}F]FV45 in the coronal section of the kidney 10 min after injection (Figure 5). This uptake could be blocked by pretreatment of valsartan, and no uptake in the kidney could be observed during the whole imaging time frame. In short, despite some unfavorable uptake into the liver (Figure 5, top), the selective uptake of [^{18}F]FV45 into renal cortex was clearly observed.

DISCUSSION

The RAS plays a key role not only in renal and cardiovascular diseases but also in processes of inflammation and cancer cell proliferation and angiogenesis. Currently, there are only a couple of AT_1-targeting PET tracers reported in the literature. Most of them are connections of easily labeled chemical moieties and the parent sartan compounds, i.e., a simple connection without paying attention to SARs of these compounds, which may significantly change the binding properties at AT_1 receptor as well as pharmacokinetics and pharmacodynamics. These factors might be crucial to reflect the true status of RAS in the body under pathophysiological conditions. Therefore, it seems necessary to develop a novel class of ^{18}F-labeled radiotracers targeting RAS through medicinal chemical techniques and applying rational drug design methodology, exemplified here with ω-fluoro-valsartan (FV45) as the first of its kind. By analyzing the SARs of sartan compounds, it was possible to design and develop compounds that retain or even improve the original ones' pharmacodynamic and pharmacokinetic properties.

Successful syntheses of the cold reference of FV45 and the corresponding precursor was achieved. The improved synthetic scheme is suitable to be scaled up, and the strategy could be applied to other sartans with similar structures, especially regarding the fluorine substitution and its position, as well as the chemical synthesis design. The introduction of fluorine would be ideal at any aliphatic moieties that bind to the same hydrophobic binding pocket of AT_1 receptor as illustrated in the SARs of losartan.[32] For example, losartan, candesartan, irbesartan, and olmesartan all have such aliphatic tail in their structures, where the fluorine could be introduced to produce PET tracer following the same strategy. The radiolabeling of FV45 was carried out under no-carrier-added K[^{18}F]F/Kryptofix$_{2.2.2}$ condition using dry acetonitrile as solvent. Good yields, as well as high purity, could be achieved within the short-time labeling procedure, which might also serve as a standard labeling procedure for other sartan tracers derived from comparable principles due to their structural similarity.

Competitive binding assay proved that FV45 has similar binding affinity (17.4 nM) to the AT_1 receptor as angiotensin II (2.0 nM) and its lead valsartan (14.0 nM). In PET imaging studies in rats, clear and fast kidney uptake was observed after administration of [^{18}F]FV45. Renal imaging instead of cardiac imaging was performed because the distribution of AT_1 receptors in the kidney is highly conserved in all mammals, whereas in the rat heart, only low density of AT_1 receptors is expressed in the atrial and ventricular myocardium.[43] Furthermore, the uptake in the kidney could be blocked by pretreatment of its parent compound—the selective AT_1 antagonist valsartan. It confirmed not only the specificity of FV45, but also our strategy to evolve AT_1 PET tracers from clinically used sartans with the minimum chemical modification. It is noteworthy that the tracer has a relatively short retention time in the kidneys, as can be seen from the dynamic scan. We do not consider this as a negative property for a novel designed tracer though: no obvious decomposition and/or metabolism happens in vivo, and no free fluorine-18 is released into the circulation system or long-term bone marrow storage (Figure 5). Approximately 15 min after tracer injection, [^{18}F]FV45 was washed out of the kidneys. This corresponds to one key point in our compound design that excretion from kidneys might be increased compared to the lead compound valsartan, or both sartan tracers mentioned above. The following two factors should be taken into account to give reasonable explanations for these changes: (a) metabolism and excretion in rodents are on average faster than in humans and (b) the relatively more polar structure of valsartan in comparison to other AT_1 antagonists makes it quickly excreted in the urine. This faster excretion might be influenced by the structural modification, i.e., the fluorination, since valsartan has an average half-life of around 6 h. The advantage of the fast excretion decreases the possibility of its accumulation in body and the consequent side effects. However, the strategy provided a basis for further tracer development, such as using alternative sartans with naturally longer half-life, which might be helpful to improve this property.

Furthermore, AT_1 antagonists also have the therapeutic potential, in particular, enhancing immunotherapy in cancer.[44] As a consequence, a PET tracer, such as [^{18}F]FV45, might also be used in investigating RAS functions in oncology, e.g., in diagnosis of cancers. It could also be helpful in answering questions like whether AT_1 antagonists could interfere in the newly discovered ACE2/Ang-(1-7)/Mas axis of the RAS.[45] In addition, provided that the iodine derivative of a sartan, such as ^{131}I instead of ^{18}F retains similar properties in vitro and in vivo, such compounds might hold potential for application in cancer therapy. Moreover, such modification derived from the clinically used sartans with the least structural changes might also provide novel directions in AT_1 antagonist development with regard to better pharmacokinetics and pharmacodynamics.

CONCLUSIONS

The first of a new generation of PET tracers derived from clinically used AT_1 receptor antagonists targeting the RAS system with minimum structural modification has been designed, successfully synthesized, and evaluated both in vitro and in vivo. Fluorine-18 instead of carbon-11 was selected for radiolabeling due to its longer half-life and advantages in precursor design. The labeling procedure has been optimized with good yield and high radiochemical purity suitable for mass production. As bioisostere of hydrogen, fluorine could be introduced into the aliphatic tail of sartans without affecting the binding affinity. As a result, [^{18}F]FV45 showed almost identical AT_1 receptor binding affinity as its lead compound valsartan. An imaging study using Wistar rats showed fast and clear kidney uptake, which could be blocked selectively by pretreatment with the AT_1 antagonist valsartan. Overall, the strategy of evolving novel PET tracers from clinically used sartans with the least structural changes may point out a new direction in RAS imaging and even facilitate translational work to humans, exemplified here with valsartan derived tracer [^{18}F]FV45 that showed almost identical affinity in binding assay and good imaging properties of kidneys in rats. The work of this paper has been included in and filed as patent.[46]

DOI: 10.1021/acsomega.8b01885
ACS Omega 2018, 3, 10460−10470

EXPERIMENTAL SECTION

Common reagents and solvents were obtained from commercial suppliers and were used without any further purification. Tetrahydrofuran (THF) was distilled from sodium/benzophenone under argon atmosphere. The reaction progress was monitored by using analytical thin-layer chromatography on precoated silica gel GF254 plates (Macherey-Nagel GmbH & Co. KG, Düren, Germany) and spots were detected under UV light (λ = 254 nm) or by staining with iodine. NMR spectra were performed with a Bruker AV-400 NMR instrument (Bruker, Karlsruhe, Germany) in [D_6]DMSO or $CDCl_3$. Chemical shifts are expressed in parts per million relative to $CHCl_3$/dimethyl sulfoxide (DMSO) (d = 7.26/2.50 and 77.16/39.52 ppm for ^{1}H- and ^{13}C NMR spectroscopy, respectively). For purity and reaction analyzes, analytical HPLC analysis was performed with a system from Shimadzu equipped with a DGU-20A3R controller, LC20AB liquid chromatograph, and an SPD-20A UV/Vis detector. Stationary phase was a Synergi 4 μm fusion-RP (150 × 4.6 mm^2) column (Phenomenex, Aschaffenburg, Germany). As mobile phase, H_2O (phase A) and methanol (phase B) were used with 1 mL/min (conc. B: 5 → 90% from 0 to 8 min; 90% from 8 to 13 min; 90 → 5% from 13 to 15 min; 5% from 15 to 18 min). All target compounds were confirmed with purity over 95%. Electrospray ionization (ESI) mass spectral data were acquired with a Shimadzu LCMS-2020.

(*S*)-*tert*-Butyl 3-Methyl-2-(((2′-(1-trityl-1*H*-tetrazol-5-yl)-[1,1′-biphenyl]-4-yl)methyl)amino)butanoate (7). 2-Tetrazol(2-trityl)-4′-methylbromide-biphenyl **4** (2.00 g, 3.59 mmol), *tert*-butyl (2*S*)-2-amino-3-methylbutanoate hydrochloride **6** (753 mg, 3.59 mmol), and *N*,*N*-diisopropylethylamine (DIPEA) (1.25 mL, 7.18 mmol) in toluene were stirred overnight at 65 °C under argon atmosphere. The solvent was removed under vacuum, and the crude product was purified by column chromatography (petroleum ether/ethyl acetate, 10:1). The coupling compound was obtained as a light yellow oil (671 mg, 53%). ESI-MS: 650.2 m/z [M + H]$^+$. ^{1}H NMR (400 MHz, $CDCl_3$) δ: 7.94−7.91 (m, 1H), 7.49−7.39 (m, 3H), 7.35−7.24 (m, 9H), 7.14−7.07 (m, 4H), 6.94−6.91 (m, 6H), 3.60 (dd, 2H, J = 3.63 Hz), 2.89 (d, 1H, J = 2.89 Hz), 1.93−1.88 (m, 1H), 1.51 (s, 9H), 0.96 (dd, 6H, J = 0.96 Hz) ppm; ^{13}C NMR (101 MHz, $CDCl_3$) δ: 174.86, 164.40, 142.51, 141.58, 140.01, 139.30, 131.01, 130.57, 130.54, 130.15, 129.43, 128.48, 127.95, 127.91, 127.63, 126.74, 83.16, 67.85, 52.59, 32.03, 28.54, 19.67, 18.96 ppm.

(*S*)-Benzyl 3-Methyl-2-(((2′-(1-trityl-1*H*-tetrazol-5-yl)-[1,1′-biphenyl]-4-yl)methyl)amino)butanoate (21). The corresponding benzyl ester was synthesized analogously to *tert*-butyl ester as described above. ESI-MS: 684.3 m/z [M + H]$^+$. ^{1}H NMR (400 MHz, $CDCl_3$) δ: 7.85−7.83 (m, 1H), 7.41−7.36 (m, 2H), 7.30−7.20 (m, 9H), 7.18−7.14 (m, 7H), 7.01−6.96 (m, 4H), 6.83−6.81 (m, 5H), 5.11 (s, 2H), 3.50 (dd, 2H, J = 3.52 Hz), 3.00 (d, 1H, J = 2.99 Hz), 1.89−1.84 (m, 1H), 0.84 (dd, 6H, J = 0.85 Hz) ppm; ^{13}C NMR (101 MHz, $CDCl_3$) δ: 175.02, 164.09, 142.16, 141.26, 139.85, 138.52, 135.91, 130.70, 130.27, 130.23, 130.20, 129.86, 129.15, 128.61, 128.43, 128.37, 128.30, 128.19, 127.70, 127.65, 127.61, 127.37, 126.42, 82.87, 66.96, 66.31, 52.27, 40.88, 31.70, 19.39, 18.61 ppm.

Benzyl 5-Chlorovalerate (13). 5-Chlorovaleric acid **5** (1 g, 7.3 mmol) and benzyl bromide (867 μL, 7.3 mmol) were dissolved in acetonitrile. Sodium carbonate was added to the above solution. The mixture was heated to reflux under argon for 15 h. The reaction solution was cooled and concentrated under vacuum. The residue was diluted with diethyl ether (30 mL) and washed with water (10 mL) and then brine (10 mL). The organic phase was dried over sodium sulfate and concentrated under vacuum to afford the product as a colorless oil (1.65 g, 100%), which was used in the next step.

Benzyl 5-Iodovalerate (14). Benzyl 5-chlorovalerate **13** (3.17 g, 13.98 mmol) was dissolved in acetone. Sodium iodide (2.60 g, 17.35 mmol) was added to the solution. This mixture was heated to reflux under argon for 5 h. The formed white solid was filtered off and the filtrate was removed under vacuum. The residue was diluted with diethyl ether (30 mL) and washed with water (10 mL) and then brine (10 mL). The organic phase was dried over sodium sulfate and concentrated under vacuum to afford the product as a colorless oil (3.51 g, 79%). ^{1}H NMR (400 MHz, $CDCl_3$) δ: 7.38−7.34 (m, 5H), 5.12 (s, 2H), 3.18 (t, 2H, J = 3.18 Hz), 2.39 (t, 2H, J = 2.39 Hz), 1.88−1.74 (m, 4H) ppm; ^{13}C NMR (101 MHz, $CDCl_3$) δ: 173.04, 136.07, 128.73, 128.41, 128.37, 66.43, 33.23, 32.84, 25.92, 5.85 ppm.

Benzyl 5-(Tosyloxy)pentanoate (15). To the cooled solution of benzyl 5-iodovalerate **14** (3.6 g, 11.3 mmol) in acetonitrile (10 mL) was added silver tosylate (3.46 mg, 12.4 mmol). The resulting solution was protected from light (aluminum foil) and stirred at room temperature overnight. The solid was filtered off. The solvent was removed under vacuum. The residue was diluted with ethyl acetate and water. The organic phase was separated, and the aqueous phase was extracted with ethyl acetate. The organic phases were combined, washed with brine, and dried over anhydrous sodium sulfate. The solvent was removed, and the residue was purified by column chromatography (petroleum ether/ethyl acetate, 3:1). The compound was obtained as a colorless oil (2.03 g, 49.5%). ^{1}H NMR (400 MHz, $CDCl_3$) δ: 7.79−7.32 (m, 9H), 5.09 (s, 2H), 4.04−4.01 (t, 2H), 2.44 (s, 3H), 2.34−2.31 (t, 2H), 1.70−1.67 (m, 4H) ppm; ^{13}C NMR (101 MHz, $CDCl_3$) δ: 172.78, 69.88, 66.28, 33.37, 28.20, 21.63, 20.89 ppm.

5-(Tosyloxy)pentanoic Acid (17). To the solution of benzyl 5-(tosyloxy)pentanoate **15** (500 mg, 1.38 mmol) in ethanol (10 mL) was added palladium on charcoal (50 mg) under argon atmosphere. The flask was equipped with a hydrogen balloon. The gas in the flask was exchanged. After stirring vigorously for 3 h at room temperature, the catalyst was filtered off through celite and the filtrate was concentrated. The compound was obtained as a colorless oil (360 mg, 96%). ^{1}H NMR (400 MHz, $CDCl_3$) δ: 8.56 (br. s, 1H), 7.79−7.77 and 7.35−7.33 (m, 2H), 4.05−4.02 (m, 2H), 2.44 (s, 3H), 2.33−2.30 (m, 2H), 1.71−1.65 (m, 4H) ppm; ^{13}C NMR (101 MHz, $CDCl_3$) δ: 178.82, 69.83, 33.04, 28.11, 21.62, 20.61 ppm.

(*S*)-*tert*-Butyl 3-Methyl-2-(5-(tosyloxy)-*N*-((2′-(1-trityl-1*H*-tetrazol-5-yl)-[1,1′-biphenyl]-4-yl)methyl)-pentanamido)butanoate (10). The solution of 5-(tosyloxy)-pentanoic acid **17** (100.5 mg, 0.37 mmol) in dry THF (5 mL) was cooled with an ice/water bath under argon atmosphere. Oxylyl chloride (32 μL, 0.37 mmol) was added to the cooled solution, followed by a catalytic amount of DMF (4.75 mg, 5 μL, 0.065 mmol). The solution was stirred for 10 min in ice/water bath and then in room temperature for 3 h. The solution was concentrated under vacuum. After adding dry THF (5 mL) and DIPEA (80.4 μL, 0.31 mmol), the solution was cooled again with the ice/water bath. A solution of compound **7** (200 mg, 0.31 mmol) in dry THF (5 mL) was added dropwise to the above solution. The reaction temperature was allowed to rise to room temperature and stirred overnight. The reaction solution was diluted with ethyl acetate and water. The organic phase was

DOI: 10.1021/acsomega.8b01885
ACS Omega 2018, 3, 10460−10470

separated and the aqueous phase was extracted with ethyl acetate. The combined organic phases were washed with brine and dried over anhydrous sodium sulfate. The compound was obtained after concentration and purification via column chromatography (petroleum ether/ethyl acetate, 3:1) as a yellow oil (100 mg, 36%). ESI-MS: 926.4 m/z $[M + Na]^+$. ^1H NMR (400 MHz, $CDCl_3$) δ: 7.80−7.62 (m, 3H), 7.44−7.36 (m, 3H), 7.22−7.19 (m, 14H), 7.05−6.86 (m, 7H), 4.74−4.30 (m, 3H), 3.99 and 3.82 (dt, 2H, J = 3.82 Hz), 2.47−1.92 (m, 3H), 2.34 (s, 3H), 1.68−1.67 (m, 2H), 1.44−1.41 (m, 2H), 1.22−1.20 (d, 9H), 0.91−0.75 (m, 6H) ppm; ^{13}C NMR (101 MHz, $CDCl_3$) δ: 171.16, 164.15, 146.90, 141.32, 133.11, 130.79, 130.21, 129.81, 129.53, 129.27, 128.29, 128.22, 128.08, 127.94, 127.90, 127.67, 127.26, 127.23, 125.73, 82.88, 81.59, 70.29, 60.40, 32.79, 27.82, 27.71, 23.85, 21.61, 21.04, 14.20 ppm.

Benzyl 5-Fluorovalerate (16). The mixture of benzyl 5-(tosyloxy)pentanoate **15** (500 mg, 1.38 mmol), potassium fluoride (80 mg, 1.38 mmol), and 18-crown-6 (364 mg, 1.38 mmol) in dry DMF (10 mL) was stirred overnight at 115 °C. The solvent was removed under vacuum. The residue was diluted with water and extracted with ethyl acetate. The combined organic phases were washed with brine, dried over sodium sulfate, and concentrated. The crude product was purified by column chromatography (petroleum ether/ethyl acetate, 10:1). The fluoride compound was obtained as a colorless oil (40 mg, 14%). ^1H NMR (400 MHz, $CDCl_3$) δ: 7.37−7.34 (m, 5H), 5.12 (s, 2H), 4.52−4.37 (dt, 2H), 2.44−2.40 (t, 2H), 1.81−1.70 (m, 4H) ppm; ^{13}C NMR (101 MHz, $CDCl_3$) δ: 173.21, 136.13, 128.71, 128.38, 128.34, 84.52, 82.88, 66.37, 33.86, 29.98, 29.79, 21.00, 20.95 ppm.

5-Fluorovaleric Acid (19). The hydrogenation was performed with benzyl 5-fluorovalerate **16** (62 mg, 0.29 mmol) in the presence of palladium on charcoal (6 mg) in ethanol. After three times of degasification, the mixture was stirred overnight. The catalyst was filtered off, and the filtrate concentrated to obtain compound **19** as a colorless volatile oil (13 mg, 37%). ^1H NMR (400 MHz, $CDCl_3$) δ: 10.85 (br. s, 1H), 4.54−4.40 (dt, 2H), 2.45−2.42 (t, 2H), 1.81−1.76 (4H) ppm; ^{13}C NMR (101 MHz, $CDCl_3$) δ: 179.49, 84.35, 82.71, 33.42, 29.75, 29.55, 20.60, 20.55 ppm.

(*S*)-Benzyl 2-(5-Fluoro-*N*-((2′-(1-trityl-1*H*-tetrazol-5-yl)-[1,1′-biphenyl]-4-yl)methyl)pentanamido)-3-methylbutanoate (22). To the solution of 5-fluorovaleric acid **19** (60 mg, 0.5 mmol) in dry dichloromethane (5 mL) was added oxalyl chloride (51 μL, 0.6 mmol). The solution was cooled using ice/water bath under argon atmosphere. Dry DMF (5 μL) was added to the above solution and then stirred at room temperature for 2 h. This solution was transferred with a syringe and added slowly to a precooled solution of compound **21** (324, 0.5 mmol) and DIPEA (130 μL, 0.75 mmol) in dry dichloromethane (5 mL). Ice/water bath was removed after the addition, and the resulting solution was stirred at room temperature overnight. Water was added to the reaction solution. The organic phase was separated, dried over dry sodium sulfate, and concentrated under vacuum. The residue was purified by column chromatography (petroleum ether/ethyl acetate, 5:1). The compound was obtained as a yellow oil (125 mg, 32%). ESI-MS: 786.4 m/z $[M + H]^+$. ^1H NMR (400 MHz, $CDCl_3$) δ: 7.80−7.75 (m, 1.4H), 7.40−7.35 (m, 3H), 7.27−7.16 (m, 23H), 7.10−7.08 (m, 1H), 6.97−6.95 (m, 4H), 6.89−6.87 (m, 11H), 4.83−4.69 (m, 3H), 4.59−4.49 (m, 2H), 4.37−4.26 (m, 3H), 4.17−4.14 (m, 1.5H), 3.95−3.92 (m, 0.5H), 2.30−2.24 (m, 1H), 2.16−2.06 (dt, 2H), 1.61−1.42 (m, 4H), 0.89 (d, 3H), 0.80 (d, 3H) ppm; ^{13}C NMR (101 MHz, $CDCl_3$) δ: 173.71, 170.31, 164.16, 141.57, 141.33, 140.27, 135.64, 135.49, 130.71, 130.45, 130.22, 129.97, 129.57, 129.06, 128.49, 128.27, 127.88, 127.67, 125.70, 84.64, 83.01, 82.91, 66.68, 63.11, 60.40, 49.35, 32.66, 31.90, 28.24, 22.53, 21.05, 20.17, 19.11, 14.21 ppm.

(*S*)-2-(*N*-((2′-(1*H*-Tetrazol-5-yl)-[1,1′-biphenyl]-4-yl)-methyl)-5-fluoropentanamido)-3-methylbutanoic Acid (FV45). To the solution of compound **21** in methanol was added palladium/charcoal. The resulting mixture was stirred vigorously under hydrogen atmosphere at room temperature overnight. The catalyst was filtered and the filtrate was concentrated under vacuum. The residue was dissolved in dry dichloromethane followed by formic acid. The solution was stirred at room temperature for 2 h. The reaction solution was concentrated under vacuum. The residue was purified via column chromatography using petroleum ether/ethyl acetate/formic acid (1:1:0.05) as the eluent system. The target cold compound was obtained as a colorless oil (48 mg, 45%). ESI-MS: 454.3 m/z $[M + H]^+$. ^1H NMR (400 MHz, $CDCl_3$) δ: 7.98−7.96 (m, 1H), 7.60−7.44 (m, 3H), 7.17−7.11 (m, 3H), 6.97−6.95 (m, 1H), 4.90 and 4.31 (dd, 2H), 4.53 and 4.41 (dt, 2H), 4.02 and 3.68 (dd, 1H), 2.63−2.39 (m, 3H), 1.87−1.73 (m, 4H), 0.98 (d, 3H), 0.94 (d, 3H) ppm; ^{13}C NMR (101 MHz, $CDCl_3$) δ: 176.33, 172.74, 154.60, 140.31, 139.25, 135.19, 131.31, 131.09, 130.31, 130.23, 129.91, 128.85, 128.42, 128.15, 127.67, 122.99, 84.67, 83.04, 77.22, 53.47, 33.81, 29.82, 29.63, 26.83, 21.33, 21.29, 19.83, 19.49, 19.15, 18.53 ppm.

Radiochemistry. $[^{18}F]F^-$ produced via proton bombardment of $H_2{}^{18}O$ was isolated by trapping on Sep-Pak Light QMA cartridge, followed by washing with 3 mL of water. Fluoride was eluted with a solution of K_2CO_3 in 0.3 mL of water (50.6 mM) into a sealed glass vial containing a solution of Kryptofix $_{2.2.2}$ (14 mg) in 0.7 mL of acetonitrile. Azeotropic drying of the solution was performed under argon flow at 120 °C with several times of addition of dry acetonitrile. The solution of 5 mg of precursor compound **10** in 0.3 mL of dry acetonitrile was added to the residue, followed by heating at 110 °C for 10 min under argon atmosphere. Subsequent hydrolysis of *tert*-butyl ester together with the removal of trityl protection group was performed in the same vessel by the addition of 0.3 mL of 1 N HCl and continued heating at 110 °C for 20 min. The mixture was cooled, diluted with 1 mL of a mixture solution of water and acetonitrile (1:1), and applied to the semipreparative HPLC column (ZORBAX Eclipse XDB-C_{18}, 5 μm, 9.4 × 250 mm^2, linear gradient of 50−95% methanol with 0.1% formic acid, 3 mL/min). After purification, 5 mL of water was added to the collected solution containing radioactive tracer. The solution was then passed through a Sep-Pak plus cartridge (C18), washed with 4 mL of water, and eluted with 3 mL of diethyl ether. The organic solution was concentrated at 50 °C and diluted with saline to an appropriate concentration for the imaging studies.

Competitive Binding Study. The radioligand binding assay was performed by using cell membrane preparations from CHO-K1 cells expressing human AT_1 receptors (Membrane Target Systems; PerkinElmer, Waltham, MA). Human AT_1 receptor (0.6 μg of membrane protein/well) was incubated with assay buffer (50 mM Tris·HCl, 5 mM $MgCl_2$, pH 7.4) containing various concentrations of test compounds (radiotracer) and ^{125}I-Sar^1-Ile^8-AngII (final concentration, 0.3 nM) in 200 μL total volume in 96-well plate at room temperature. After 1 h, the plate was washed nine times with 250 μL/well of wash buffer (50 mM Tris·HCl, pH 7.4) to remove unbound tracer.

DOI: 10.1021/acsomega.8b01885
ACS Omega 2018, 3, 10460−10470

Membrane-bound radioactivity was counted using a γ-counter (FH 412; Frieseke & Höpfner, Erlangen, Germany). Nonspecific binding of ^{125}I-Sar^1-Ile^8-AngII was estimated in the presence of 10 M unlabeled AngII. Specific binding is defined as total binding minus nonspecific binding. K_i values are calculated from the IC_{50} values using the Cheng−Prusoff equation: $K_i = IC_{50}/(1 + [L]/K_d)$, where the final concentration of radioligand is 0.03 nM and K_d of ^{125}I-Sar^1-Ile^8-AngII is 0.16 nM.

Animal Imaging Study. Healthy male Wistar rats (weighing 200−250 g) were used. The animal protocols were approved by the local institutional animal care and use committee and were conducted strictly according to the Guide for the Care and Use of Laboratory Animals.[47] The rats were maintained under anesthesia by 2% isoflurane during the whole experiment. [^{18}F]FV45 (20−25 MBq) was administered via the tail vein as two different medications: intravenous injection of the tracer (n = 3); a pretreatment of 30 mg/kg valsartan orally 3 h before the study and 10 min intravenous before tracer delivery. Imaging was performed using a dedicated small-animal PET system (Inveon, Siemens Healthcare). A 60 min list-mode PET acquisition was started shortly after injection. The reconstructed PET images were analyzed using an imaging-processing application (AMIDE-bin, version 1.0.2).

■ ASSOCIATED CONTENT

Supporting Information

The Supporting Information is available free of charge on the ACS Publications website at DOI: 10.1021/acsomega.8b01885.

SMILES strings of chemical compounds (CSV)

HPLC data of target compound; HPLC data showing γ signal after radiolabeling procedure (PDF)

■ AUTHOR INFORMATION

Corresponding Authors

*E-mail: michael.decker@uni-wuerzburg.de. Tel: +49(931)31-89676 (M.D.).

*E-mail: thiguchi@me.com. Tel: +49(931)201-35455 (T.H.).

ORCID

Michael Decker: 0000-0002-6773-6245

Notes

The authors declare the following competing financial interest(s): Patent application (EP 18150613.0) for 18F-labeled sartans as novel PET tracers targeting angiotensin II type 1 receptor (X.C., T.H., M.D., and M.H.).

All applicable international, national, and/or institutional guidelines for the care and use of animals were followed. No human participants were involved in this study.

■ ACKNOWLEDGMENTS

This study was funded by German Research Council (DFG grant CH 1516/2-1 and HI 1789/3-3). It was also supported by the Competence Network of Heart Failure funded by the Integrated Research and Treatment Center (IFB) of the Federal Ministry of Education and Research (BMBF). Funding was also received from the European Union's Horizon 2020 research and innovation programme under the Marie Skłodowska-Curie grant agreement No. 701983.

■ REFERENCES

(1) Tamargo, M.; Tamargo, J. Future drug discovery in renin-angiotensin-aldosterone system intervention. *Expert Opin. Drug Discovery* **2017**, *12*, 827−848.

(2) Ma, T. K. W.; Kam, K. K. H.; Yan, B. P.; Lam, Y. Y. Renin-angiotensin-aldosterone system blockade for cardiovascular diseases: Current status. *Br. J. Pharmacol.* **2010**, *160*, 1273−1292.

(3) McMurray, J. J.; Packer, M.; Desai, A. S.; Gong, J.; Lefkowitz, M. P.; Rizkala, A. R.; Rouleau, J. L.; Shi, V. C.; Solomon, S. D.; Swedberg, K.; Zile, M. R. PARADIGM-HF Investigators and Committees. Angiotensin-neprilysin inhibition versus enalapril in heart failure. *N. Engl. J. Med.* **2014**, *371*, 993−1004.

(4) Passos-Silva, D. G.; Brandan, E.; Santos, R. A. Angiotensin as therapeutic targets beyond heart disease. *Trends Pharmacol. Sci.* **2015**, *36*, 310−320.

(5) Mao, Y.; Xu, X.; Wang, X.; Zheng, X.; Xie, L. Is angiotensin-converting enzyme inhibitors/angiotensin receptor blockers therapy protective against prostate cancer? *Oncotarget* **2016**, *7*, 6765−6773.

(6) Zhang, J.; Liu, J.; Chen, J.; Li, X.; Wu, Y.; Chen, H.; Wu, W.; Zhang, K.; Gu, L. Angiotensin receptor blockers (ARBs) reduce the risk of lung cancer: a systematic review and meta-analysis. *Int. J. Clin. Exp. Med.* **2015**, *8*, 12656−12660.

(7) Zhang, W.; Liang, Z.; Li, J.; Cai, S. Angiotensin receptor blockers use and the risk of lung cancer: A meta-analysis. *J. Renin-Angiotensin-Aldosterone Syst.* **2015**, *16*, 768−773.

(8) Lee, L. D.; Mafura, B.; Lauscher, J. C.; Seeliger, H.; Kreis, M. E.; Gröne, J. Antiproliferative and apoptotic effects of telmisartan in human colon cancer cells. *Oncol. Lett.* **2014**, *8*, 2681−2686.

(9) Vinson, G. P.; Barker, S.; Puddefoot, J. R. The renin-angiotensin system in the breast and breast cancer. *Endocr.-Relat. Cancer* **2012**, *19*, R1−R19.

(10) Côrtes, S. F.; Lemos, V. S.; Corriu, C.; Stoclet, J. C. Changes in angiotensin II receptor density and calcium handling during proliferation in SHR aortic myocytes. *Am. J. Physiol.* **1996**, *271*, H2330−H2338.

(11) Iyer, S. N.; Raizada, M. K.; Katovich, M. J. AT1 receptor density changes during development of hypertension in hyperinsulinemic rats. *Clin. Exp. Hypertens.* **1996**, *18*, 793−810.

(12) Reja, V.; Goodchild, A. K.; Philips, J. K.; Pilowsky, P. M. Upregulation of angiotensin AT1 receptor and intracellular kinase gene expression in hypertensive rats. *Clin. Exp. Pharmacol. Physiol.* **2006**, *33*, 690−695.

(13) Crowley, S. D.; Gurley, S. B.; Coffman, T. M. AT1 receptors and control of blood pressure: the kidney and more. *Trends Cardiovasc. Med.* **2007**, *17*, 30−34.

(14) Chen, X.; Werner, R. A.; Javadi, M. S.; Maya, Y.; Decker, M.; Lapa, C.; Herrmann, K.; Higuchi, T. Radionuclide imaging of neurohormonal system of the heart. *Theranostics* **2015**, *5*, 545−558.

(15) Wollenweber, T.; Bengel, F. M. Cardiac molecular imaging. *Semin. Nucl. Med.* **2014**, *44*, 386−397.

(16) Kobayashi, R.; Chen, X.; Werner, R. A.; Lapa, C.; Javadi, M. S.; Higuchi, T. New horizons in cardiac innervation imaging: introduction of novel 18F-labeled PET tracers. *Eur. J. Nucl. Med. Mol. Imaging* **2017**, *44*, 2302−2309.

(17) Wegman-Ostrosky, T.; Soto-Reyes, E.; Vidal-Millán, S.; Sánchez-Corona, J. The renin-angiotensin system meets the hallmarks of cancer. *J. Renin-Angiotensin-Aldosterone Syst.* **2015**, *16*, 227−233.

(18) Mathews, W. B.; Yoo, S. E.; Lee, S. H.; Scheffel, U.; Rauseo, P. A.; Zober, T. G.; Gocco, G.; Sandberg, K.; Ravert, H. T.; Dannals, R. F.; Szabo, Z. A novel radioligand for imaging the AT1 angiotensin receptor with PET. *Nucl. Med. Biol.* **2004**, *31*, 571−574.

(19) Zober, T. G.; Mathews, W. B.; Seckin, E.; Yoo, S. E.; Hilton, J.; Xia, J.; Sandberg, K.; Ravert, H. T.; Dannals, R. F.; Szabo, Z. PET imaging of the AT1 receptor with [^{11}C]KR31173. *Nucl. Med. Biol.* **2006**, *33*, 5−13.

(20) Higuchi, T.; Fukushima, K.; Xia, J.; Mathews, W. B.; Lautamäki, R.; Bravo, P. E.; Javadi, M. S.; Dannals, R. F.; Szabo, Z.; Bengel, F. M. Radionuclide imaging of angiotensin II type 1 receptor upregulation after myocardial ischemia-reperfusion injury. *J. Nucl. Med.* **2010**, *51*, 1956−1961.

(21) Antoun, R. Characterization of [^{11}C]methyl-losartan as a Novel Radiotracer for PET Imaging of the AT$_1$ Receptor. M.S. Thesis, Faculty of Medicine, University of Ottawa: Ottawa, Canada, 2011.

DOI: 10.1021/acsomega.8b01885
ACS Omega 2018, 3, 10460−10470

(22) Arksey, N. Synthesis and Preliminary Evaluation of an F-18 Labeled Fluoropyridine Losartan Analogue as a Novel PET Tracer for Imaging AT_1 Receptors. M.S. Thesis University of Ottawa Heart Institute: Ottawa, Canada, 2012.
(23) Arksey, N.; Hadizad, T.; Ismail, B.; Hachem, M.; Valdivia, A. C.; Beanlands, R. S.; deKemp, R. A.; DaSilva, J. N. Synthesis and evaluation of the novel 2-[18F]fluoro-3-propxy-triazole-pyridine-substituted losartan for imaging AT1 receptors. *Bioorg. Med. Chem.* **2014**, *22*, 3931−3937.
(24) Hachem, M. Characterization of [^{18}F]FPyKYNE-losartan as a Novel PET Tracer for Imaging AT_1 Receptors. M.S. Thesis, University of Ottawa Heart Institute: Ottawa, Canada, 2015.
(25) Hadizad, T.; Collins, J.; Antoun, R. E.; Beanlands, R. S.; DaSilva, J. N. [^{11}C]Methyl-losartan as a potential ligand for PET imaging angiotensin II AT_1 receptors. *J. Labelled Compd. Radiopharm.* **2011**, *54*, 754−757.
(26) Hachem, M.; Tiberi, M.; Ismail, B.; Hunter, C. R.; Arksey, N.; Hadizad, T.; Beanlands, R. S.; deKemp, R. A.; DaSilva, J. N. Characterization of 18F-FPyKYNE-Losartan for imaging AT1 receptors. *J. Nucl. Med.* **2016**, *57*, 1612−1617.
(27) Gulaldi, N. C.; Xia, J.; Feng, T.; Hong, K.; Mathews, W. B.; Ruben, D.; Kamel, I. R.; Tsui, B. M.; Szabo, Z. Modeling of the renal kinetics of the AT1 receptor specific PET radioligand [^{11}C]KR31173. *Biomed. Res. Int.* **2013**, No. 835859.
(28) Feng, T.; Tsui, B. M.; Li, X.; Vranesic, M.; Lodge, M. A.; Gulaldi, N. C.; Szabo, Z. Image-derived and arterial blood sampled input functions for quantitative PET imaging of the angiotensin II subtype 1 receptor in the kidney. *Med. Phys.* **2015**, *42*, 6736−6744.
(29) Fukushima, K.; Bravo, P. E.; Higuchi, T.; Schuleri, K. H.; Lin, X.; Abraham, M. R.; Xia, J.; Mathews, W. B.; Dannals, R. F.; Lardo, A. C.; Szabo, Z.; Bengel, F. M. Molecular hybrid positron emission tomography/computed tomography imaging of cardiac angiotensin II type 1 receptors. *J. Am. Coll. Cardiol.* **2012**, *60*, 2527−2534.
(30) Ismail, B.; deKemp, R. A.; Croteau, E.; Hadizad, T.; Burns, K. D.; Beanlands, R. S.; DaSilva, J. N. Treatment with enalapril and not diltiazem ameliorated progression of chronic kidney disease in rats, and normalized renal AT1 receptor expression as measured with PET imaging. *PLoS One* **2017**, *12*, No. e0177451.
(31) Abraham, I.; MacDonald, K.; Hermans, C.; Aerts, A.; Lee, C.; Brié, H.; Vancayzeele, S. Real-world effectiveness of valsartan on hypertension and total cardiovascular risk: review and implications of a translational research program. *Vasc. Health Risk Manage.* **2011**, *7*, 209−235.
(32) Santella, J. B.; Duncia, J. V.; Ensinger, C. L.; VanAtten, M. K.; Carini, D. J.; Wexler, R. R.; Chiu, A. T.; Wong, P. C.; Timmermans, P. B. M. W. M. Balanced angiotensin II receptor antagonists. III. The effects of substitution at the imidazole 5-position. *Bioorg. Med. Chem. Lett.* **1994**, *4*, 2235−2240.
(33) Beutler, U.; Boehm, M.; Fuenfschlling, P. C.; Heinz, T.; Mutz, J. P.; Onken, U.; Mueller, M.; Zaugg, W. A high-throughput process for valsartan. *Org. Process Res. Dev.* **2007**, *11*, 892−898.
(34) Nakashima, A.; Kawashita, H.; Masuda, N.; Saxer, C.; Niina, M.; Nagae, Y.; Iwasaki, K. Identification of cytochrome P450 forms involved in the 4-hydroxylation of valsartan, a potent and specific angiotensin II receptor antagonist, in human liver microsomes. *Xenobiotica* **2005**, *35*, 589−602.
(35) Amantini, D.; Beleggia, R.; Fringuelli, F.; Pizzo, F.; Vaccaro, L. TBAF-catalyzed synthesis of 5-substituted 1*H*-tetrazole under solvent-less conditions. *J. Org. Chem.* **2004**, *69*, 2896−2898.
(36) Agelis, G.; Resvani, A.; Durdagi, S.; Spyridaki, K.; Tumová, T.; Slaninová, J.; Giannopoulos, P.; Vlahakos, D.; Liapakis, G.; Mavromoustakos, T.; Matsoukas, J. The discovery of new potent non-peptide Angiotensin II AT1 receptor blockers: a concise synthesis, molecular docking studies and biological evaluation of N-substituted 5-butylimidazole derivatives. *Eur. J. Med. Chem.* **2012**, *55*, 358−374.
(37) Solladié-Cavallo, A.; Bencheqroun, M. Inexpensive reagents for the synthesis of amides from esters and for regioselective opening of epoxides. *J. Org. Chem.* **1992**, *57*, 5831−5834.
(38) Shalom, E.; Takrouri, K.; Metsuyanim, N.; Grufi, A.; Katzhendler, J.; Srebnik, M. Semiautomated synthesis of a novel [^{18}F] amine fluorocyanoborane for PET imaging studies. Radiosynthesis and in vivo characterization in rats. *Appl. Radiat. Isot.* **2007**, *65*, 204−208.
(39) Kornblum, N.; Jones, W. J.; Anderson, G. J. A new and selective method of oxidation. The conversion of alkyl halides and alkyl tosylates to aldehydes. *J. Am. Chem. Soc.* **1959**, *81*, 4113−4114.
(40) Badone, D.; Jommi, G.; Pagliarin, R.; Tavecchia, P. Use of polyethylene glycol in the synthesis of alkyl fluorides from alkyl sulfonates. *Synthesis* **1987**, *1987*, 920−921.
(41) Meanwell, N. A. Fluorine and fluorinated motifs in the design and application of bioisosteres for drug design. *J. Med. Chem.* **2018**, 5822.
(42) Werner, R. A.; Wakabayashi, H.; Chen, X.; Hirano, M.; Shinaji, T.; Lapa, C.; Rowe, S. P.; Javadi, M. S.; Higuchi, T. Functional renal imaging with 2-deoxy-2-^{18}F-fluorosorbitol PET in rat models of renal disorders. *J. Nucl. Med.* **2018**, *59*, 828−832.
(43) Allen, A. M.; Zhuo, J.; Mendelsohn, F. A. O. Localization and function of angiotensin AT1 receptors. *Am. J. Hypertens.* **2000**, *13*, 31S−38S.
(44) Pinter, M.; Jain, R. K. Targeting the renin-angiotensin system to improve cancer treatment: Implications for immunotherapy. *Sci. Transl. Med.* **2017**, *9*, No. eaan5616.
(45) Santos, R. A. S.; Sampaio, W. O.; Alzamora, A. C.; Motta-Santos, D.; Alenina, N.; Bader, M.; Campagnole-Santos, M. J. The ACE2/Angiotensin-(1-7)/MAS axis of the renin-angiotensin system: focus on angiotensin-(1-7). *Physiol. Rev.* **2018**, *98*, 505−553.
(46) Chen, X.; Decker, M.; Higuchi, T.; Hoffmann, M. Sartan Analogue. EP18150613.0, 2018.
(47) National Research Council. *Guide for the Care and Use of Laboratory Animals*, 8th ed.; National Academies Press: Washington (DC), 2011.

DOI: 10.1021/acsomega.8b01885
ACS Omega 2018, 3, 10460−10470